

^3He : Does the problem persists?

L. Guzman-Ramirez^{1*}, J. E. Pineda¹, A. A. Zijlstra¹, R. Stancliffe² and A. Karakas³

¹Jodrell Bank Centre for Astrophysics, School of Physics and Astronomy, University of Manchester, Manchester, M13 9PL, UK

²Argelander-Institut für Astronomie, Auf dem Hügel 71, D-53121 Bonn, Germany

³Research School of Astronomy & Astrophysics, Mt Stromlo Observatory, Canberra, Australia

Accepted 2013 March 20. Received 2013 March 14; in original form 2013 February 25

ABSTRACT

To understand the chemical evolution of the Galaxy, we need to understand the contribution of PNe in the ^3He abundance. ^3He abundances have been detected only in a couple of PNe, their abundances are consistent with the standard models, in which ^3He is produced in significant quantities by stars of 1–2 M_{\odot} . However, for all the other PNe observed to date there have been no detections, therefore only upper limits in their abundance can be calculated. Observations of the $^3\text{He}^+$ emission line using the VLA towards the PNe IC 418, NGC 6572 and NGC 7009 were used to obtain upper limits for their ^3He abundance. Because the abundance of ^3He in H II regions, the ISM and the proto-solar system is much lower than what is predicted, new chemical models were proposed. The resulting evolution of ^3He , based on stellar evolution models, can be consistent with the values determined in pre-solar material and the ISM if 96% of the population of stars with mass below $\sim 2.5M_{\odot}$ has undergone enhanced ^3He depletion. This implies that unless the combined sample of PNe that has been observed so far is very atypical, the solution to the “The ^3He Problem” lies elsewhere. However, the results presented here suggest that more observations are needed in order to make a strong conclusion about the stellar evolution models.

Key words: circumstellar matter – radio: abundances, planetary nebulae.

1 INTRODUCTION

The cosmic abundance of the ^3He isotope has important implications for many fields of astrophysics. It impacts stellar evolution, chemical evolution and cosmology. The present interstellar ^3He abundance, as per all the light elements, comes from a combination of Big Bang Nucleosynthesis (BBN) and stellar nucleosynthesis (Wilson & Rood 1994). H II regions are young objects compared with the age of the Galaxy, so they represent the zero-age objects. Their ^3He abundance is the result of 13.7Gyr of Galactic chemical evolution. Any hydrogen-burning zone of a star which is not sufficiently hot ($>7\times 10^6\text{K}$) will produce ^3He via the p - p chain. Stars with masses $<2.5M_{\odot}$ are the net producers of ^3He . For these stars, p - p burning is rapid enough to produce D *in situ*, and enable the production of ^3He ($\text{D} + \text{p} \rightarrow ^3\text{He} + \gamma$). More massive stars are dominated by CNO burning; although they do produce some ^3He via the p - p chain in their outer zones, it is not enough to offset the ^3He destruction in the interior zones (Dearborn et al. 1986). Therefore PNe evolved from stars with masses $<2.5M_{\odot}$ should be substantially enriched in ^3He . PNe ^3He abundances are important tests of stellar evolution theory (Bania et al. 2010).

Galli et al. (1995) presented “The ^3He Problem”. According to standard models of stellar nucleosynthesis there should be a $^3\text{He}/\text{H}$

abundance gradient in the Galactic Disk with the highest abundances occurring in the highly-processed inner Galaxy, the $^3\text{He}/\text{H}$ abundance should grow with source metallicity and the protosolar $^3\text{He}/\text{H}$ value should be less than what is found in the present ISM.

After more than 30 years of effort, observations of the abundance of ^3He in H II regions are inconsistent with these expectations (Rood et al. 1979; Bania et al. 2007). For the ^3He problem to be solved, it will require that the vast majority of low-mass stars fail to enrich the ISM. One suggestion to solve this is adding extra mixing in the red giant branch (RGB) stage. This extra mixing adds to the standard first dredge-up to modify the surface abundances. Eggleton et al. (2006) showed that mixing in the surface convective zone of low-mass stars in the RGB phase is extended below the classical convective limit and that it is very fast compared with the nuclear time scales of either the hydrogen-burning shell or the ^3He -burning shell. Their model estimated that as the H-shell burns outwards the ^3He will be destroyed. Although low-mass stars do produce considerable amounts of ^3He on the main sequence phase, this will be all destroyed by the substantially deeper mixing they expect to occur in the red giant branch phase. These same results estimate that while 90% of the ^3He is destroyed in 1 M_{\odot} stars, only 40-60% is destroyed in a 2 M_{\odot} star model, depending on the speed of mixing. For stars above 4 M_{\odot} , the bottom of the convective envelope is hot enough for nuclear burning (hot bottom burning). This leaves a mass range around 2 M_{\odot} which is still expected to con-

* E-mail: lizette.ramirez@postgrad.manchester.ac.uk

tribute to ^3He enrichment. Recent observations of Smiljanic et al. (2009) have further complicated the issue: they found a few 2.5–4 M_{\odot} stars with low $^{12}\text{C}/^{13}\text{C}$ ratios, where CN-processed material has been brought from the H-shell to the envelope. Extra mixing mechanisms do not appear to operate in these stars, and additional mechanisms are assumed. Whether these would affect ^3He is not known.

The abundance of ^3He can only be derived from measurements of the hyperfine transition of $^3\text{He}^+$ which has a rest frequency of 8.665 GHz. Detecting $^3\text{He}^+$ in PNe challenges the sensitivity limits of all existing radio telescopes. The detection of ^3He in any PN will require $^3\text{He}/\text{H} \sim 10^{-4}$, which is the abundance predicted by standard stellar models. After an intense search of ^3He in PNe, the results are still unclear. Bania et al. (2010) observed a sample of 12 PNe. ^3He was detected in only 2 of them. NGC 3242 was observed with Effelsberg a 100m dish from the Max Planck Institute for Radio Astronomy (MPIfR) and the NRAO 140-foot telescopes, however the observations are inconsistent with each other, implying a $^3\text{He}/\text{H}$ abundance that is $\sim 25\%$ of the 10^{-4} abundance predicted. For the case of J320, ^3He was detected at a 4σ level with the NRAO VLA. Composite $^3\text{He}^+$ average spectrum for 6 PNe (NGC 3242, NGC 6543, NGC 6720, NGC 7009, NGC 7662, and IC 289), using Effelsberg, Arecibo and *GBT* observations, consistently show $^3\text{He}^+$ emission at the $\sim 1\text{mK}$ level.

^3He is created in low mass stars and ejected during the late phases of their evolution. Galactic models predict a rapid increase over the past 5Gyr. This is however in contradiction to the observed abundances in the ISM. The cause is believed to be destruction of ^3He during the RGB phase, by hot bottom burning at higher masses and thermohaline mixing at low masses, leaving only a narrow mass range between. In this paper we present upper limits estimates for 3 PNe. The description of the observations made using the VLA in Section 2, the abundance calculations and results are presented in Section 3, the stellar models are presented in the discussion in Section 4 and the main conclusions are in Section 5.

2 OBSERVATIONS USING THE VLA

Motivated by this problem, three planetary nebulae were observed using the national radioastronomy observatory (NRAO) very large array (VLA) in D configuration. In Table 1 the targets and the parameters of the observations are presented.

The data was edited and reduced using the Common Astronomy Software Applications (CASA) package. The calibration technique was slightly different for every object due to different S/N ratio in the phase and bandpass calibrators.

- **IC 418.** For this source the phase calibrator (B0609-157) was used as a bandpass calibrator. The integration time was averaged every hour to get the bandpass solutions. The calibrator B0137+331 was used to calibrate the intensity scale. The continuum intensity of this source was sufficient to perform the standard self-calibration technique. The self-calibration algorithm was applied to the continuum after the standard phase and bandpass calibration.

Three loops of self-calibration were applied, the first 2 were only in phase, using the complete time interval for the first one and then a solutions interval of 300s. After this a self-calibration in amplitude and phase was applied using 150s for the solutions interval. Once this was obtained these solutions were applied to the line data, the continuum was subtracted and the clean image was created.

- **NGC 6572.** For this source the phase calibrator (B1751+096)

was used as a bandpass calibrator; the integration time was averaged every hour to get the bandpass solutions. The calibrator B1331+305 was used to calibrate the intensity scale. The continuum intensity of this source was sufficient to perform the standard self-calibration technique. The self-calibration algorithm was applied after the standard phase and bandpass calibration. Several loops of self-calibration were applied. The first 4 were only in phase, changing the solutions interval from using the complete integration time up to intervals of 21s. After this a self-calibration in amplitude and phase was applied three times, also changing the intervals of the solutions, starting using 150s. Ultimately the best result for the self-calibration was obtained using a solution interval of 21s in phase only and a solution interval of 30s for the amplitude and phase. Once this was obtained these solutions were applied to the line data, the continuum was subtracted and the clean image was created.

- **NGC 7009.** For this source also the phase calibrator (B2136+006) was used as a bandpass calibrator; the integration time was averaged every hour to get the bandpass solutions. The same calibrator was used to calibrate the intensity scale. For this data set, a flux calibrator was not observed. But as mentioned in Table 1 there were more observations taken for these sources. In the case of NGC 7009 a day before of the observations analysed here a flux calibrator was observed; this was used to calibrate the phase calibrator (same for both observations) and the flux obtained was imposed into the phase calibrator for the data set used here. Therefore the same calibrator was used as a phase, bandpass and amplitude calibrator. For this source a self-calibration technique was applied, but it did not improve the data. Therefore the image and spectrum presented here were made using only the standard calibration. Once this was obtained these solutions were applied to the line data, the continuum was subtracted and the clean image was created.

The continuum images are completely limited by the finite dynamic range of the strong continuum emission and thus are not limited by thermal fluctuations. The line data, after subtraction of the continuum, are limited by thermal noise. This explains why the continuum rms values are larger than the line data values (see Table 1).

3 RESULTS

The result of the observations are presented in Figure 1, showing the emission cube with the continuum subtracted. As a reference the emission of the continuum is over plotted in red contours. The spectrum presented on the right of every image is the emission coming from the centre of the contours, where the emission of the line should be. The $^3\text{He}^+$ line was not detected for any of the objects, therefore only upper limits for the density values were calculated. We used a 3σ level of the rms as an upper limit for the three sources.

The $^3\text{He}^+$ column density can be obtained using:

$$N(^3\text{He}^+) = \frac{g_l + g_u}{g_u} \frac{8\pi k\nu^2}{hc^3 A_{ul}} \int T_B(\nu) d\nu, \quad (1)$$

where $g_u = 1$ is the g value or magnetic moment of the upper state, $g_l = 3$ is the g value or magnetic moment of the lower state, $A_{ul} = 1.95436 \times 10^{-12} \text{s}^{-1}$ (Gould 1994), and $T_B(\nu)$ is the brightness temperature profile of the line. For a gaussian line profile,

$$\int T_B(\nu) d\nu = 1/2 \sqrt{\frac{\pi}{\ln 2}} T_B^0 \Delta\nu, \quad (2)$$

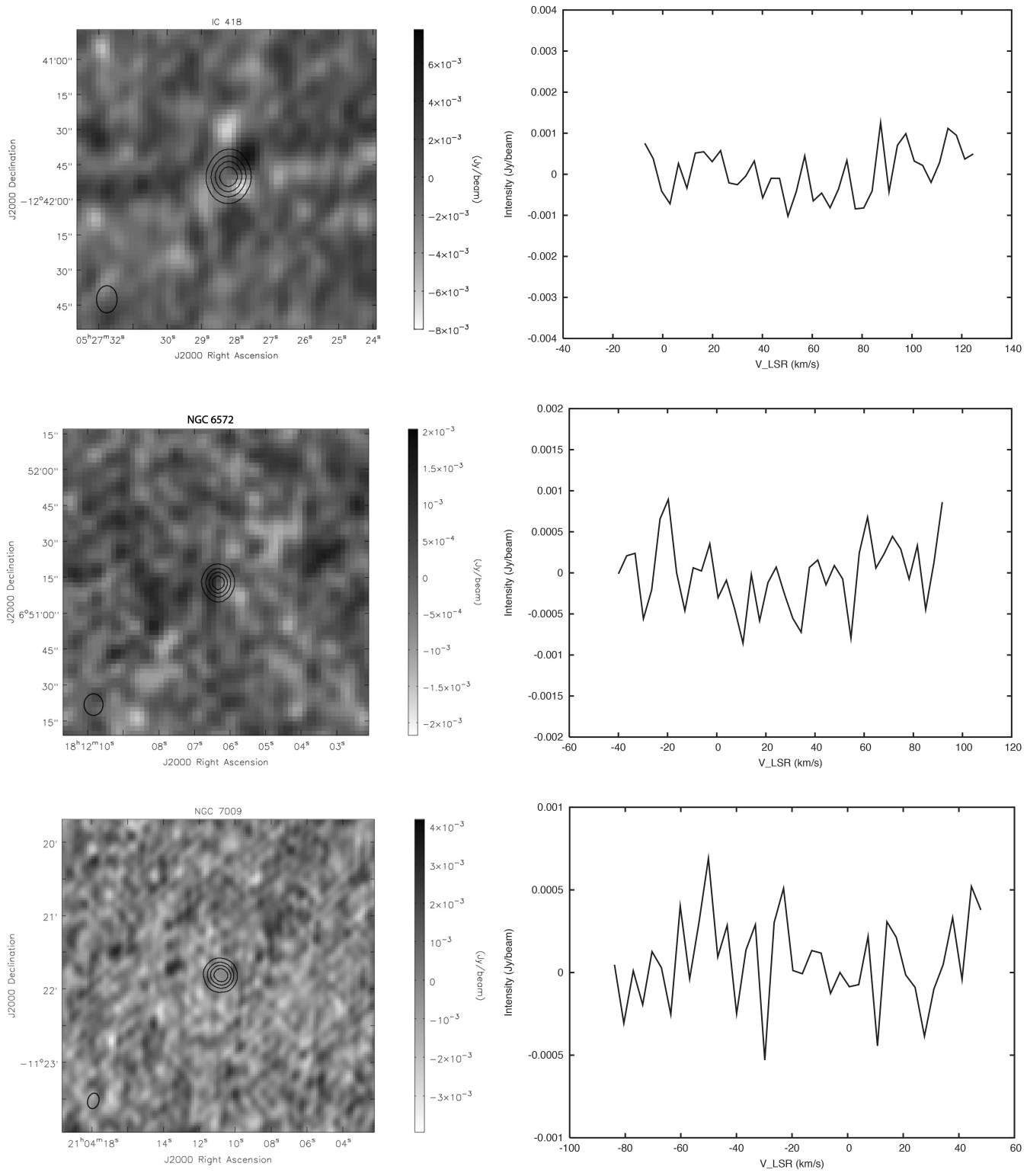


Figure 1. VLA observations of IC 418 (top), NGC 6572 (middle), and NGC 7009 (bottom). On the left side the image shows the line emission of the source, continuum subtracted. The red contours in the centre show the position of the continuum emission for each source. On the right side is the spectrum at the peak continuum position of the source. The ³He⁺ line should be at 62 km s⁻¹ for IC 418, at -8.7 km s⁻¹ for NGC 6572 and at -46.6 km s⁻¹ for NGC 7009.

Table 1. VLA Observations Parameters.

Parameters	IC418	NGC 6572	NGC 7009
Date*	15-12-2009	13-12-2009	26-12-2009
Total observed time (hr)	6	6.2	4.6
Configuration	D	D	D
R.A. (J2000)	05:27:28.20	18:12:06.36	21:04:10.8
DEC (J2000)	-12:41:50.26	+06:51:13.01	-11:21:48.25
FWHM of primary beam (arcmin)	5.4	5.4	5.4
Size of the PNe (arcsecs)	30×6	18.9×6.9	12×7
FWHM of synthesised beam (arcsec)	13	9	9
Total bandwidth (MHz)	6.152	6.152	6.152
Number of channels	62	62	62
LSR central velocity (km s ⁻¹)	62.0	-8.7	-46.6
Observed ν (MHz)	8662.6338	8665.6132	8666.0602
Spectral resolution (km s ⁻¹)	3.378	3.378	3.378
Flux density calibrator	0137+331	1331+305	1733-130
Phase calibrator	0609-157	1751+096	2136+006
Line channel rms (mJy beam ⁻¹)**	1	0.4	0.8
Continuum rms (mJy beam ⁻¹)	2.0	1.53	1.3

*More observations were obtained, due to the lack of calibrators or bad data they were not considered here.

**Continuum subtracted

where T_B^0 is the brightness temperature at the centre of the line and $\Delta\nu$ is the full width at half power. The brightness temperature T_B^0 is related to the observed beam-averaged brightness temperature T_L , by (Rood et al. 1995)

$$T_B^0 = T_L \frac{\theta_b^2 + \theta_s^2}{\theta_s^2}, \quad (3)$$

where θ_b and θ_s are the beam and source angular radii.

The number of $^3\text{He}^+$ atoms per unit volume, $n(^3\text{He}^+)$, can be obtained by dividing the column density $N(^3\text{He}^+)$ by the averaged optical path, $\langle \Delta s \rangle$, through the source. Representing a PN as a homogeneous sphere of radius $R=\theta_s D$, where D is the distance, the optical path at a position angle θ is $\Delta s(\theta) = 2\sqrt{R^2 - (\theta D)^2}$, and the optical path averaged on the source results $\langle \Delta s \rangle = \pi R/2 = \pi\theta_s D/2$.

The expression for $n(^3\text{He}^+)$ is then

$$n(^3\text{He}^+) = 8 \sqrt{\frac{\pi}{\ln 2}} \frac{g_l + g_u}{g_u} \frac{kv^2}{hc^3 A_{ul}} \frac{\theta_b^2 + \theta_s^2}{D\theta_s^3} T_L \Delta\nu. \quad (4)$$

Rearranging Equation 4 and using the numerical values, the final expression can be presented as follows,

$$n(^3\text{He}^+) = 22.7 \left(\frac{T_L}{\text{mK}} \right) \left(\frac{\Delta\nu}{\text{km s}^{-1}} \right) \left(\frac{D}{\text{kpc}} \right)^{-1} \left(\frac{\theta_s}{\text{arcsec}} \right)^{-3} \left(\frac{\theta_b}{41''} \right)^2 \left(1 + \frac{\theta_s^2}{\theta_b^2} \right) \text{cm}^{-3} \quad (5)$$

Table 2 shows the calculated $^3\text{He}^+$ density using Equation 5 for the three sources. The distance values used were 1.2kpc for NGC 7009 (Galli et al. 1997), 1.2kpc for NGC 6572 (Hajian et al. 1995) and 1.3kpc for IC 418 (Guzmán et al. 2009). To calculate the abundance we need to divide by the H^+ density. The H^+ values presented in Table 2 were taken from Galli et al. (1997); Balser et al. (2006); Morisset & Georgiev (2009) for NGC 7009, NGC 6572 and IC 418 respectively. The H^+ abundance is derived from the thermal free-free bremsstrahlung radio continuum emission, and is proportional to the square of the density. To obtain these values, the PNe were modelled using a numerical code, called NEBULA

for the case of NGC 6572 and NGC 7009. This code calculates the radio recombination line and continuum emission from an ionised plasma. The modelled nebulae are composed solely of hydrogen and helium. The numerical grid uses a three-dimensional Cartesian coordinate system that allows for the specification of a completely arbitrary density and ionisation structure. For the case of IC 418 its H^+ abundance was modelled using Cloudy_3D (Morisset 2006).

Once we calculated the $^3\text{He}^+/\text{H}^+$ abundance, we can compare the values with the theoretical calculations and the stellar models predictions.

Figure 2 shows the ^3He abundance of the three PNe from this work, they are presented using the red symbols. The mass values used are 1.7 ± 0.3 for IC 418 (Morisset & Georgiev 2009), 1.0 ± 0.2 for NGC 6572 (Hyung et al. 1994) and 1.4 ± 0.2 for NGC 7009 (Galli et al. 1997). For comparison the PNe from Balser et al. (1997) are also presented (using green symbols), where the mass estimates are from Galli et al. (1997). All these measurements represent upper limits points. For all the $^3\text{He}^+/\text{H}^+$ values calculated and taken from the literature it has been assumed that $^3\text{He}/\text{H} \approx ^3\text{He}^+/\text{H}^+$ (Balser et al. 1994).

PNe IC 418 and NGC 7009 have values consistent with Population I and II theoretical predictions. For IC 418, this is the first upper limit calculation and it agrees with the stellar model predictions. For NGC 7009 a $^3\text{He}/\text{H}$ abundance of $< 8.24 \times 10^{-3}$ was calculated. Previous observations of this source gave estimates of $< (5.8 - 31) \times 10^{-4}$, therefore our estimated value does not improve earlier estimates. In the case of NGC 6572 the abundance calculated is lower than the theoretical models predict. An upper limit for this PNe was calculated by Balser et al. (2006): the value they estimate is $< 10^{-3}$. We found an upper limit of $< 2.4 \times 10^{-4}$.

4 DISCUSSION

The stellar evolution models are also presented in Figure 2. The curves labelled as Pop I and II show the standard abundance of ^3He taken from Weiss et al. (1996). The Big Bang line is the primordial value of $^3\text{He}/\text{H}$.

In order to understand the chemical evolution of the Galaxy, it

Table 2. Parameters used to calculate the ³He abundance in the PNe.

PNe	D (kpc)	M (M _⊙)	T _L (mK)	Δv (km s ⁻¹)	n(H ⁺) (cm ⁻³)	n(³ He ⁺) (cm ⁻³)	³ He ⁺ /H ⁺ (10 ⁻³)
IC 418	1.3	1.7±0.3 ¹	27	30	3×10 ³	<12.99	<4.33
NGC 6572	1.2	1.0±0.2 ²	150	15	22×10 ³	<5.38	<0.24
NGC 7009	1.2	1.4±0.2 ³	465	43	3.62×10 ³	<29.85	<8.24

¹Morisset & Georgiev (2009), ²Hyung et al. (1994), ³Galli et al. (1997)

is crucial we understand the contribution of PNe to the ³He abundance. Chemical evolution models started including only processed primordial deuterium (D) as a source of ³He synthesis in low mass stars. But even without including any stellar production of ³He, these models showed that ³He/H increases with time (Vangioni-Flam et al. 1994). Because the abundance of ³He in H II regions, the ISM and the proto-solar system is much lower than predicted, new chemical models were proposed.

These models include non convective mixing processes that either prevent the buildup of ³He on the main-sequence or destroys ³He along the upper red giant branch (Boothroyd & Sackmann 1999; Lagarde et al. 2012).

The blue curve labelled ExtraMix represents the results of stellar nucleosynthesis calculations using deep mixing by Boothroyd & Sackmann (1999). The detailed calculations indicate that the mass dependence of the destruction of ³He is very strong, and the resulting abundance decreases sharply for masses below ~2.5M_⊙. It is clearly seen in this Figure that the observed PNe have not suffered any depletion. Almost all of the PNe are more than a factor of ~2 above the non-standard curve (the Extramix predictions).

One suggestion to solve this is by adding some additional mixing mechanism during the first ascent of the RGB. By allowing material to circulate below the convective envelope after the first dredge-up has occurred, the surface abundances can be modified as the star approaches the tip of the RGB. Observationally, the existence of this non-convective mixing is well established (e.g. Gratton et al. 2000) as carbon, lithium and the ¹²C/¹³C ratio are all observed to change as stars reach the tip of the RGB. That this process should also affect the ³He abundance seems clear as to affect these elements and isotopes one must reach temperatures where ³He burning reactions will occur. However, the physical cause of this non-convective mixing has proven elusive and many possible mechanisms, such as rotation (e.g. Palacios et al. 2006) have been suggested.

The hydrodynamic simulations of Eggleton et al. (2006) pointed to a particularly convenient process for this extra mixing. Their simulations showed that a mean molecular weight inversion caused by the destruction of ³He could drive circulation of material. This process (subsequently identified with thermohaline convection by Charbonnel & Zahn 2007a) would allow low-mass stars to destroy the ³He that they produce during the main sequence phase.

Newer stellar models from Lagarde et al. (2012) analyse the evolution of ³He and its destruction due to the effects of thermohaline instability and rotation-induced mixing. Their models show that thermohaline mixing can induce significant depletion of ³He in low- and intermediate-mass stars. Although these stars remain the net producers of ³He, their contribution to the Galactic evolution of this element is highly reduced compared to classical theory. It is claimed in their paper that thermohaline mixing is the only physical mechanism known so far able to solve the so-called “The ³He Problem”. Importantly, its inhibition by a fossil magnetic field in

red giant stars that are descendants of Ap stars does reconcile the measurements of ³He/H in Galactic H II regions with high values of ³He in a few PNe.

We have used the STARS stellar evolution code (Eggleton 1971; Pols et al. 1995; Stancliffe & Eldridge 2009) to produce a set of stellar models in the mass range 1-3.5 solar masses at intervals of 0.25 solar masses and with a metallicity of Z=0.02. These models have been computed from the pre-main sequence to the first thermal pulse on the asymptotic giant branch. Thermohaline mixing has been included at all stages of the evolution using the diffusive formalism of Ulrich (1972) and Kippenhahn et al. (1980). Following the work of Charbonnel & Zahn (2007a), we set the free parameter of the formalism to C_t = 1000, a value which not only reproduces the compositional changes in field giants, but which has also been shown to reproduce the difference in behaviour between C-normal and C-rich metal-poor stars (Stancliffe et al. 2009) as well as the abundance changes in globular cluster stars (Angelou et al. 2011). Note that this value is not supported by current hydrodynamical simulations of thermohaline mixing (Traxler et al. 2011; Denissenkov & Merryfield 2011) and that some other process (or processes) could be the cause of abundance changes on the giant branch (e.g. magnetic fields, Charbonnel & Zahn 2007b; Nordhaus et al. 2008). These stellar models using thermohaline mixing are also represented in Figure 2 (light-blue line).

As shown in Figure 2 the ³He abundance of two PNe (NGC 6572 and NGC 6720) fall below the line that the model predicts, therefore at least for these two PNe the thermohaline mixing model fails to reproduce their ³He abundances.

5 CONCLUSIONS

Upper-limits for the ³He abundance of three PNe have been estimated using the ³He⁺ emission line observed with the VLA towards the PNe IC 418, NGC 6572 and NGC 7009. In total one strong detection (PN J320) and seven upper limits of the ³He abundance on PNe have been reported in the literature, including this work, and are consistent with standard stellar evolution calculations. These estimates are two orders of magnitude larger than what is found in H II regions (Balser et al. 1997), the local ISM (Gloeckler & Geiss 1996) and the proto-solar system (Geiss 1993).

The resulting evolution of ³He is only consistent with the values determined in pre-solar material and the ISM if more than 96% of the whole population of stars with mass below ~2.5M_⊙ have undergone enhanced ³He depletion. These results suggest that more observations are needed in order to make a strong conclusion about the stellar evolution models.

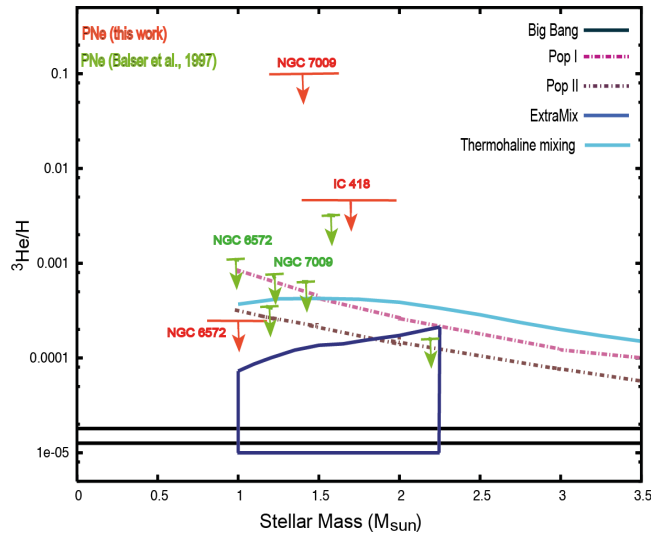


Figure 2. Abundance of $^3\text{He}/\text{H}$ versus main-sequence masses. The red symbols represent the work from this paper. The horizontal bar represents the mass range of the progenitor star. The green symbols represent the sample of 6 PNe (NGC 3242, NGC 6543, NGC 6720, NGC 7009, NGC 7662 and IC 289) from Balser et al. (1997), using the mass estimates from Galli et al. (1997). The curves as Pop I and II show the standard abundance of ^3He taken from Weiss et al. (1996). The blue curve labelled ExtraMix represents the results of stellar nucleosynthesis calculations using deep mixing by Boothroyd & Sackmann (1999). The light-blue curve represent the stellar models using thermohaline mixing. The Big Bang line is the primordial value of $^3\text{He}/\text{H}$.

ACKNOWLEDGMENTS

This work is based on observations made with the VLA from NRAO, PI A. Zijlstra. LGR and AZ acknowledge the support of CONACyT (Mexico). Astrophysics at Manchester is supported by grants from the STFC. JEP has received funding from the European Communitys Seventh Framework Programme (FP7/2007-2013) under grant agreement No 229517. RJS is the recipient of a Sofja Kovalevskaja Award from the Alexander von Humboldt Foundation.

REFERENCES

- Angelou G. C., Church R. P., Stancliffe R. J., Lattanzio J. C., Smith G. H., 2011, *ApJ*, 728, 79
 Balser D. S., Bania T. M., Brockway C. J., Rood R. T., Wilson T. L., 1994, *ApJ*, 430, 667
 Balser D. S., Bania T. M., Rood R. T., Wilson T. L., 1997, *ApJ*, 483, 320
 Balser D. S., Goss W. M., Bania T. M., Rood R. T., 2006, *ApJ*, 640, 360
 Bania T. M., Balser D. S., Rood R. T., Wilson T. L., LaRocque J. M., 2007, *ApJ*, 664, 915
 Bania T. M., Rood R. T., Balser D. S., 2010, in Charbonnel C., Tosi M., Primas F., Chiappini C., eds, IAU Symposium Vol. 268 of IAU Symposium, Measurements of ^3He in Galactic HII regions and planetary nebulae. pp 81–90
 Boothroyd A. I., Sackmann I.-J., 1999, *ApJ*, 510, 232
 Charbonnel C., Zahn J.-P., 2007a, *A&A*, 467, L15
 Charbonnel C., Zahn J.-P., 2007b, *A&A*, 476, L29

- Dearborn D. S. P., Schramm D. N., Steigman G., 1986, *ApJ*, 302, 35
 Denissenkov P. A., Merryfield W. J., 2011, *ApJL*, 727, L8
 Eggleton P. P., 1971, *MNRAS*, 151, 351
 Eggleton P. P., Dearborn D. S. P., Lattanzio J. C., 2006, *Science*, 314, 1580
 Galli D., Palla F., Ferrini F., Penco U., 1995, *ApJ*, 443, 536
 Galli D., Stanghellini L., Tosi M., Palla F., 1997, *ApJ*, 477, 218
 Geiss J., 1993, in Prantzos N., Vangioni-Flam E., Casse M., eds, Origin and Evolution of the Elements Primordial abundances of hydrogen and helium isotopes.. pp 89–106
 Gloeckler G., Geiss J., 1996, *Nature*, 381, 210
 Gould R. J., 1994, *ApJ*, 423, 522
 Gratton R. G., Sneden C., Carretta E., Bragaglia A., 2000, *A&A*, 354, 169
 Guzmán L., Loinard L., Gómez Y., Morisset C., 2009, *AJ*, 138, 46
 Hajian A. R., Terzian Y., Bignell C., 1995, *AJ*, 109, 2600
 Hyung S., Aller L. H., Feibelman W. A., 1994, *MNRAS*, 269, 975
 Kippenhahn R., Ruschenplatt G., Thomas H.-C., 1980, *A&A*, 91, 175
 Lagarde N., Romano D., Charbonnel C., Tosi M., Chiappini C., Matteucci F., 2012, *A&A*, 542, A62
 Morisset C., 2006, in Barlow M. J., Méndez R. H., eds, Planetary Nebulae in our Galaxy and Beyond Vol. 234 of IAU Symposium, Cloudy_3D, a new pseudo-3D photoionization code. pp 467–468
 Morisset C., Georgiev L., 2009, *A&A*, 507, 1517
 Nordhaus J., Busso M., Wasserburg G. J., Blackman E. G., Palmerini S., 2008, *ApJL*, 684, L29
 Palacios A., Charbonnel C., Talon S., Siess L., 2006, *A&A*, 453, 261
 Pols O. R., Tout C. A., Eggleton P. P., Han Z., 1995, *MNRAS*, 274, 964
 Rood R. T., Bania T. M., Wilson T. L., Balser D. S., 1995, in Crane P., ed., The Light Element Abundances The Quest for the Cosmic Abundance of ^3He . p. 201
 Rood R. T., Wilson T. L., Steigman G., 1979, *ApJL*, 227, L97
 Smiljanic R., Gauderon R., North P., Barbay B., Charbonnel C., Mowlavi N., 2009, *A&A*, 502, 267
 Stancliffe R. J., Church R. P., Angelou G. C., Lattanzio J. C., 2009, *MNRAS*, 396, 2313
 Stancliffe R. J., Eldridge J. J., 2009, *MNRAS*, 396, 1699
 Traxler A., Garaud P., Stellmach S., 2011, *ApJL*, 728, L29
 Ulrich R. K., 1972, *ApJ*, 172, 165
 Vangioni-Flam E., Olive K. A., Prantzos N., 1994, *ApJ*, 427, 618
 Weiss A., Wagenhuber J., Denissenkov P. A., 1996, *A&A*, 313, 581
 Wilson T. L., Rood R., 1994, *Annual Review of Astron and Astrophys*, 32, 191

This paper has been typeset from a $\text{\TeX}/\text{\LaTeX}$ file prepared by the author.